General Synthesis Methodology for Acoustic Wave Ladder Filters in the Bandpass Domain

Santi Cano, *Graduate Student Member, IEEE*, Carlos Caballero, *Graduate Student Member, IEEE*, Omar Barrera, *Senior Member, IEEE*, Ruochen Lu, *Senior Member, IEEE*, Jordi Verdú, *Senior Member, IEEE*, and Pedro de Paco, *Senior Member, IEEE*

***Abstract*—In designing acoustic wave (AW) ladder filters, synthesis methods utilize the lowpass prototype (LP) representation to analyze bandpass responses in the normalized domain. This technique reduces the filter's polynomial order and achieves asymmetric responses by incorporating frequency-invariant reactance (FIR) elements. While this technique is particularly effective for narrowband filter designs, it faces limitations with wideband filters due to errors that arise when transforming extracted LP elements to the bandpass domain. There are different approaches for the exact modeling of AW ladder filters in the real frequency domain. However, current direct bandpass (DB) techniques for AW ladder filters cannot be generalized, as they lack flexibility in characterizing frequency-dependent input and output (I/O) phases and suffer from numerical issues during parameter extraction due to excessively large polynomial coefficients in high-order or narrowband filter designs. This work aims to address both problems: first, to generalize the DB methodology for AW ladder filters by computing the transfer function while considering the asymptotic behavior at both the origin and infinity, as well as controlling the frequency-dependent I/O phases through complex reflection zeros (CRZs). Second, to enhance numerical accuracy during parameter extraction by relying on precise root-finding methods rather than interpolated coefficients. To validate the effectiveness of the proposed DB approach, the synthesized model has been compared with a manufactured $LiNbO_3$ thin-film AW ladder filter, which features a wide fractional bandwidth (FBW) of 18% and demonstrates excellent agreement between the simulated and measured responses. Finally, an 18th-order AW ladder filter has been synthesized to validate numerical stability even for narrowband filters.**

***Index Terms*—Acoustic-wave filters, bandpass domain, frequency transformation error, lowpass prototype (LP), narrowband approximation, reduced Chebyshev (RC), wideband filters.**

I. Introduction

MOBILE communications have emerged as one of the most spectrum-demanding services, making radio frequency (RF) filtering a critical aspect of mobile devices. Acoustic wave (AW) filters provide an essential solution for addressing the complexities of filtering and spectrum control in the RF interface due to their unbeatable contribution in miniaturization and quality factor [1], [2], [3]. These filters are typically implemented either as standalone devices for single-band responses in TDD access [4] or as components of more complex networks, such as duplexers or multiplexers, connected to a common antenna node to satisfy carrier aggregation (CA) schemes [5], [6]. Recent advancements in wireless communication standards, particularly 5G and Wi-Fi, have introduced new wideband frequencies that enhance data rates, low latency, and network capacity not achievable in previously implemented RF front ends [7], [8]. Among the most important 5G wideband are the n77 (3.3–4.2 GHz), n78 (3.3–3.8 GHz), and n79 (4.4–5.0 GHz) bands, which are part of the ultrahigh-band (UHB) spectrum. On the other hand, the introduction of Wi-Fi-6E (which operates from 5.925 to 7.125 GHz) expands the available spectrum to include the 6-GHz band.

However, the increasing demand for wider bandwidths limits the automatic numerical design procedure based on synthesis techniques introduced in [4], since the narrowband approximation, which makes use of the lowpass prototype (LP) approach, shows inaccuracies when synthesizing wideband filters, such as the 5G n77 BAW transversal filter of [9], the UNII-5 AW pseudo-ladder and ladder topologies of [10] or even the n77 hybrid acoustic-electromagnetic (ACEM) filter of [11]. Fig. 1(a) and (b) compares a narrowband and a wideband AW ladder filter synthesized using the LP technique from [4]. It is clearly seen that the LP approximation remains effective for narrowband filters, but when the same transfer function is scaled to a wideband filter, it introduces so many errors that it compromises the passband. Ariturk et al. [11] used a method to improve the transformation of the originally extracted pole to the Butterworth-van dyke (BVD) model of [4], establishing a relationship between the AW resonator and the coupling matrix. This method provides a more accurate representation of the frequency behavior of the extracted elements after their transformation to the bandpass domain. Nevertheless, this approach and that of [4] still rely on a narrowband approximation. To address the synthesis of such designs, a common practice in designing wideband filters is to postoptimize the input and output (I/O) elements and the first and last resonators, rather than the entire network [12]. To

Received 4 February 2025; revised 25 March 2025 and 22 April 2025; accepted 25 April 2025. This work was supported in part by the Agencia Estatal de Investigacion (AEI)–Ministerio de Ciencia e Innovación under Project PID2021-127203OB-I00 and in part by the Departament d'Universitats i Recerca. *(Corresponding author: Santi Cano.)*

Santi Cano, Carlos Caballero, Jordi Verdú, and Pedro de Paco are with the Department of Telecommunications and Systems Engineering, Universitat Autònoma de Barcelona, 08193 Barcelona, Spain (e-mail: santi.cano@uab.cat).

Omar Barrera and Ruochen Lu are with the Department of Electrical and Computer Engineering, The University of Texas at Austin, Austin, TX 78712 USA.

Digital Object Identifier 10.1109/TMTT.2025.3565809

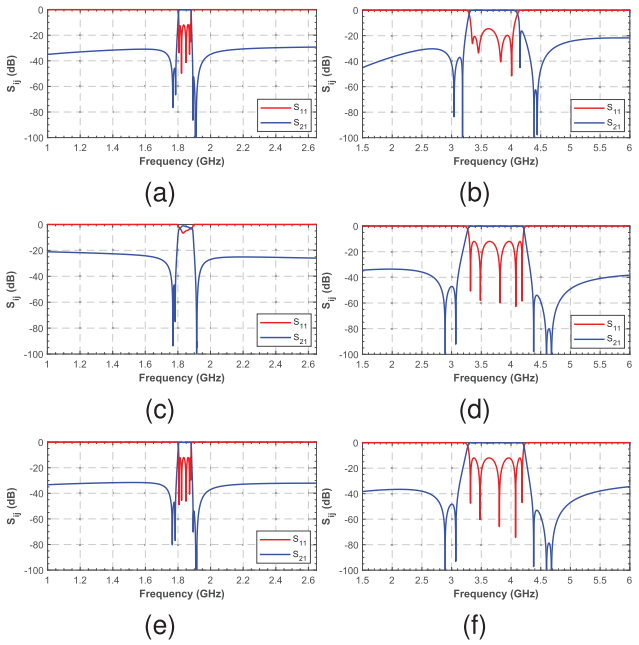

Fig. 1. Comparison of a fifth-order narrowband filter and its equivalent wideband filter synthesized using: (a) and (b) LP approximation from [4], (c) and (d) DB approach from [13], and (e) and (f) proposed DB approach.

mitigate the "frequency transformation errors," designers have observed that the majority of the error contribution originates from the I/O elements, which fundamentally dominate the asymptotes at extreme frequencies. This suggests that the frequency transformation errors are actually poor modeling of those vertical asymptotes in the LP domain.

Aiming to escape from narrowband techniques, several authors presented contributions about direct bandpass (DB) synthesis that enhance the synthesis accuracy [13], [14], [15], [16], [17], [18], [19], [20]. Amari was the first to propose in [14] a method for defining the polynomials of a transfer function directly in the real domain, being a method applicable to wideband filters because the impedance asymptotes at origin and infinity, that cannot be represented by fully canonical networks, are now considered. However, Amari formulation is not valid for AW ladder topologies because when placing a TZ at the origin, the $T_0(\omega)$ term also introduces an additional undesired reflection zero (RZ) within the passband, preventing the extraction of the AW ladder filter elements. In [15], a filtering function able to accommodate a source-load coupling was derived, introducing a TZ at the origin and no resonance in the passband. Nevertheless, when applying this methodology to AW ladder networks, an attenuation pole appears above the passband, resulting in poor out-of-band (OoB) rejection at high frequencies. More recently, Evdokimova et al. [16] combined both [14] and [15] filtering functions to overcome their respective limitations. However, in [16], AW ladder filters did not take into account the input phase correction that manages the source and load reactive elements because bandpass synthesis techniques operate with purely real coefficients. For this reason, Iuliia complemented the term $T_0(\omega)$ in [13] with a coefficient A, which introduced a phase correction that was limited into the range of 90° and it caused the uncontrolled appearance of undesired imaginary RZs at OoB frequencies. Therefore, there was no effective control over the I/O reactive elements. Moreover, this DB approach is prone to numerical errors when extracting the circuit elements because the inclusion of both negative and positive passbands doubles the admittance function order compared to the LP. These numerical errors can lead to the partial extraction of circuit elements being performed incorrectly, as shown in Fig. 1(c), or even cause the extraction process to fail before completion. This problem is aggravated when the filter has a high order or a very narrow bandwidth, since, in both cases, the polynomial coefficients become excessively large, which increases the accumulated error during the extraction process. Although the impact of round-off errors [21], [22] can be mitigated (but not entirely eliminated) by performing the extraction simultaneously from both the source and the load, a nonunitary coupling arises in the middle of asymmetric ladder networks, something undesired in AW technology. Therefore, additional tools that enhance numerical stability at the cost of increasing computational time are necessary to complete the extraction procedure from source to load, as explained in [13].

This work proposes a general synthesis methodology for AW ladder filters in the bandpass domain that overcomes the current limitations of the DB approach. This methodology establishes a mathematical connection between the poles and zeros of the LP and DB approaches using a logarithmic mapping function, incorporating the missing TZs at the origin and infinity, and controlling the OoB fly-backs by adding complex RZs (CRZs). These CRZs, which uncontrollably appeared in [13], manage the I/O phases and are implemented using reduced Chebyshev (RC) filtering functions that maintain equiripple behavior between -1 and 1 rad/s, allowing for the formulation of the DB filtering function in a flexible way. On the other hand, the proposed DB methodology ensures numerical stability for any fractional bandwidth (FBW) and filter order without the need for multiprecision tools, as shown in Fig. 1(e) and (f). To tackle round-off errors during parameter extraction, this DB approach relies on accurate roots-finding methods instead of interpolated coefficients, taking advantage of the fact that the bandpass domain roots are already available once the RC filtering function is mapped from the LP domain to the bandpass domain. The entire parameter extraction procedure is performed using a novel root-based methodology that employs an iterative vector fitting process, similar to [23], to update the roots of the numerator and denominator of the admittance function after each element extraction.

The effectiveness of the proposed DB methodology is demonstrated by comparing a synthesized third-order AW ladder filter with the experimental measurements of the manufactured $LiNbO_3$ thin-film AW filter of Barrera et al. [24], which operates between 21.35 and 25.65 GHz, and it has an FBW of 18%. Finally, a fictitious narrowband 18th-order AW ladder filter is synthesized to confirm numerical stability for any order and FBW. In addition to the high-order example, a comparison table is provided to quantify the numerical and computational time advantages of the proposed root-based method, compared to coefficient-based approaches and tools

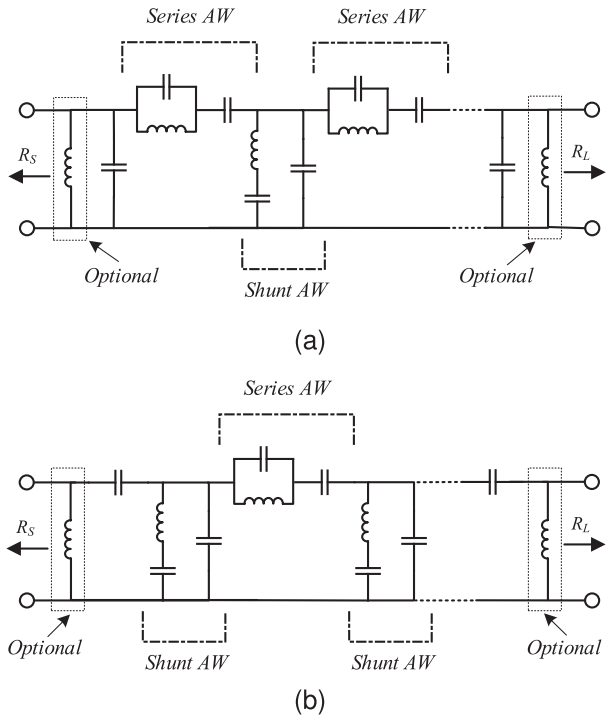

Fig. 2. Ladder network starting with a (a) series AW resonator and a (b) shunt AW resonator, and considering I/O inductances.

that allow for enhanced precision, such as Symbolic Math Toolbox [25] or the commercial tool Advanpix [26].

II. Formulation of the AW Ladder Filtering Function in the Bandpass Domain

Despite rigidity, AW Ladder filters serve as a fundamental topology due to their high performance and scalability, particularly when a high-order filter is implemented or combined with other topologies [1], [5]. This network is organized with consecutive series and parallel resonators placing upperband or lowerband transmission zeros, respectively. All resonators are treated as extracted pole sections that can be solved using analytical methods. Regarding the reactive I/O elements, they are commonly understood as impedance-matching elements that enhance the in-band filter response [27], [28] or provide higher isolation levels at the antenna port in duplexers and multiplexers [5], [6]. According to Saal and Ulbrich [29], the ladder topology can deal with an optional shunt-connected or series-connected I/O inductor that places a TZ in the origin or infinity, respectively. Moreover, a mandatory I/O capacitor prepares the extraction of the first and last resonators. This capacitor is arranged in shunt (yielding a partial extraction at infinity) if the first resonator is series, or in series (making a partial extraction at origin) if the first resonator is a shunt, as shown in Fig. 2(a) and (b), respectively. It is interesting to notice that this capacitor is often omitted in real devices and replaced with an optimized inductor that approximates it [5], [27], [30]. In view of the state of the art, this work will only focus on the definition of the filtering function when there are no inductors and when I/O shunt inductors are considered.

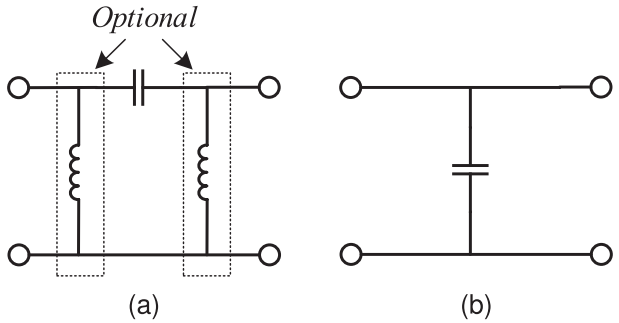

Fig. 3. Equivalent circuit model of the asymptotic behavior of the network starting in the series AW resonator at the frequency of (a) $\Omega = 0$ and (b) $\Omega = \infty$.

A. Definition of the Proposed DB Approach

Let us start by defining the S-parameters using the characteristic polynomials $P(s)$, $F(s)$, and $E(s)$ of a filter function [12] in the normalized domain $s = \Sigma + j\Omega$

$$\begin{bmatrix} S_{11}(s) & S_{12}(s) \\ S_{21}(s) & S_{22}(s) \end{bmatrix} = \frac{1}{E(s)} \begin{bmatrix} F(s)/\varepsilon_r & P(s)/\varepsilon \\ P(s)/\varepsilon & (-1)^N F(s)^*/\varepsilon_r \end{bmatrix} \quad (1)$$

where ε_r and ε are the normalization constants that ensure monic polynomials, and the roots of $P(s)$, $F(s)$, and $E(s)$ represent the TZs, RZs, and poles of the ladder topology, respectively.

Focusing on the series-starting case of Fig. 2(a), when $\Omega = 0$, three zeros are managed by the I/O shunt inductors and all series capacitors, whereas when $\Omega = \infty$, there is only 1 zero managed by shunt capacitors. Fig. 3(a) and (b) captures the information of a ladder circuit evaluated at the extreme frequencies where vertical asymptotes appear. They are neglected in the LP domain because BVD resonators and I/O elements are partially and fully modeled, respectively, by frequency-invariant reactances (FIRs), which do not account for frequency-dependent slopes [31]. Therefore, when these I/O FIRs are scaled using the bilateral transformation, uncontrolled asymptotes emerge at extreme frequencies, degrading the in-band response as the FBW increases. Table I compares the LP and the proposed DB by describing their filtering characteristics. In the case of the LP approximation, the generalized Chebyshev function is defined by a target equiripple level and N prescribed TZs (N_{TZ}), making the ladder topology a fully canonical network with $N = N_{\mathrm{TZ}}$, being N the number of AW resonators to be implemented. A generalized form of this function is computed through the recursive technique in [12] or using a more flexible Remez-like algorithm as in [32].

In contrast, the proposed DB approach modifies the LP through an intermediate step, called the extended LP (ELP), by adding CRZs that model the I/O phases through the use of RC functions [33]. In this approach, the filtering function is no longer fully canonical because $N \neq N_{\mathrm{TZ}}$, where the polynomial $F(s)$ now captures N_{CRZ} CRZs and $N - N_{\mathrm{CRZ}}$ purely imaginary in-band RZs. The CRZ position modifies the OoB fly-backs and plays a key role in controlling the I/O reactive element values as well as the static capacitances of the first and last resonators, as detailed in Section II-B. The number of CRZs

TABLE I
COMPARISON BETWEEN THE MAIN CHARACTERISTICS OF THE LP AND DB MODELS

Domain	LP approximation	ELP before applying the mapping function	DB approach
Order	N	$N+1$ without considering $L_{I/O}$ $N+2$ considering $L_{I/O}$	$2N+2$ without considering $L_{I/O}$ $2N+4$ considering $L_{I/O}$
Transmission Zeros	N TZ at $\Omega \notin [-1,1]$ 0 TZ at $\Omega=\infty$ 0 TZ at $\Omega=0$	N TZ at $\Omega \notin [-1,1]$ 1 TZ at $\Omega=\infty$ without considering $L_{I/O}$ 2 TZ at $\Omega=\infty$ considering $L_{I/O}$ 0 TZ at $\Omega=0$	N TZ at $\Omega \in \{-\infty,-1\} \cup \{-\frac{\omega_1}{\omega_2},0\}$ N TZ at $\Omega \in \{0,\frac{\omega_1}{\omega_2}\} \cup \{1,\infty\}$ 1 TZ at $\Omega=\infty$ 1 TZ at $\Omega=0$ without considering $L_{I/O}$ 3 TZ at $\Omega=0$ considering $L_{I/O}$
Phase Control	2 constant I/O phases at $\{\theta_{11},\theta_{22}\} \in \{-180,180\}^\circ$	1 CRZ without considering $L_{I/O}$ 1 pair of conjugated CRZs considering $L_{I/O}$	1 pair of conjugated RZs without considering $L_{I/O}$ 2 pairs of conjugated CRZ considering $L_{I/O}$
Filtering Function	Generalized chebyshev (GC)	Reduced Chebyshev (RC)	ELP mapped to a dual band symmetric around 0

depends on whether I/O inductors are considered: one CRZ is used when they are not considered, while a conjugated pair of CRZs is employed if they are taken into account. Finally, an extra TZ at $\Omega = 0$ is included to fully define the ladder transfer function by mapping all zeros and poles of the LP response, which lies between $\Omega = [-1, 1]$ rad/s, into the real domain using a Hermitian function that preserves the same information in both the positive and negative frequency planes. Consequently, the new passband is symmetric around 0, but it may be asymmetric with respect to the center frequency. To accomplish this, a logarithmic mapping function [34] is used, increasing the filter order to $N_{\mathrm{DB}} = 2N + 4$ with three TZs at origin when I/O inductors are considered or $N_{\mathrm{DB}} = 2N + 2$ with only one TZ at origin if they are not. Therefore, to obtain the roots $\{\Omega'_{\mathrm{TZ}}\}$ and $\{\Omega'_{\mathrm{RZ}}\}$ of the polynomials $P(s)$ and $F(s)$, respectively, in the real frequency domain, the logarithmic mapping function is defined as follows:

$$\begin{cases} \Omega = 1 + k_L \log_{10}(-\Omega'), & k_L = \frac{2}{\log_{10}(-fc_2/fc_1)} \\ \Omega = 1 + k_U \log_{10}(\Omega'), & k_U = \frac{2}{\log_{10}(fc_2/fc_1)} \end{cases} \tag{2}$$

where k_L and k_U are the normalized cut-off frequencies in the logarithmic domain, Ω is the frequency variable in the single-band domain, and Ω' the frequency variable in the dual-band domain, in such a way that $\Omega(\Omega') = \pm 1$ for $\Omega' = [-1, -fc_1/fc_2; fc_1/fc_2, 1]$. Fig. 4 shows the frequency behavior of the polynomial magnitude responses of three AW ladder filters synthesized with the LP and DB before and after applying the logarithmic mapping function illustrated in Fig. 5. It can be seen how the OoB rejection of the LP approximation remains infinitely constant, and when the asymptotes at infinity are modeled, it decreases monotonically toward the origin and $\pm\infty$.

It should be noted that this mapping function introduces a small distortion in the $F(s)$ polynomial that increases linearly as the equiripple approaches the lower band edge of the mapped band. This equiripple loss becomes more pronounced as the slope of the function toward the origin becomes steeper. Consequently, this equiripple loss is more noticeable when inductors are included, as they have three TZs at the origin instead of one. This small distortion can be easily recovered by combining the RC with a nonequiripple function [35] and tuning the extreme points Ω_i using a set of scaling factors α_i, as it is depicted in Fig. 5.

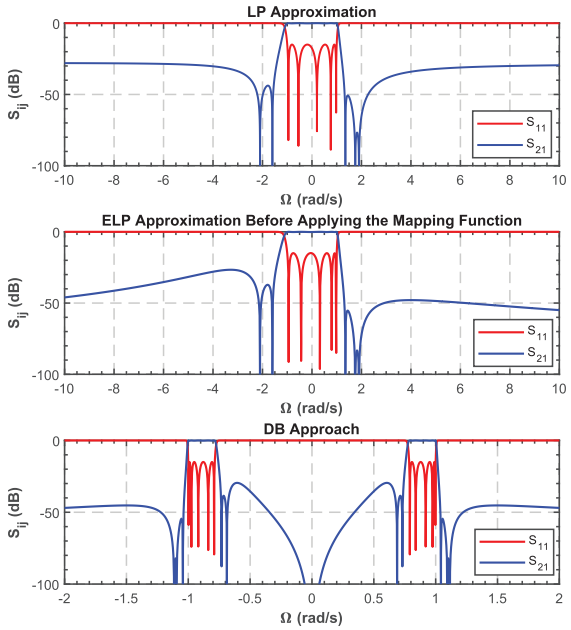

Fig. 4. Polynomial magnitude comparison between the LP approximation and the proposed DB approach before and after applying the mapping function.

To enhance clarity, the DB approach proposed in this section has been summarized as a four-step process.

Step 1: Generate the RC equiripple transfer function by incorporating N_{CRZ}, based on the details provided in the middle column of Table I. The characteristic function $C_{eq}(\Omega)$ oscillates with a constant amplitude Δ_{eq}, with its extreme points Ω_i located at the maximums

$$\left|C_{eq}(\Omega)\right|_{\Omega=\Omega_i} = \left|\frac{F(\Omega)}{P(\Omega)}\right|_{\Omega=\Omega_i} = |\Delta_{eq}|. \tag{3}$$

Step 2: Map the single-band RC transfer function, which is equiripple, to the normalized real frequency domain using (2) and add one or three TZs at the origin as necessary, depending on the presence or absence of I/O inductors. Adding a TZ at the origin means including it into the array of mapped finite Ω'_{TZ}. At this point, the mapped function $C(\Omega')$ accounts for the TZs at both the origin and infinity, but it has now become a nonequiripple function.

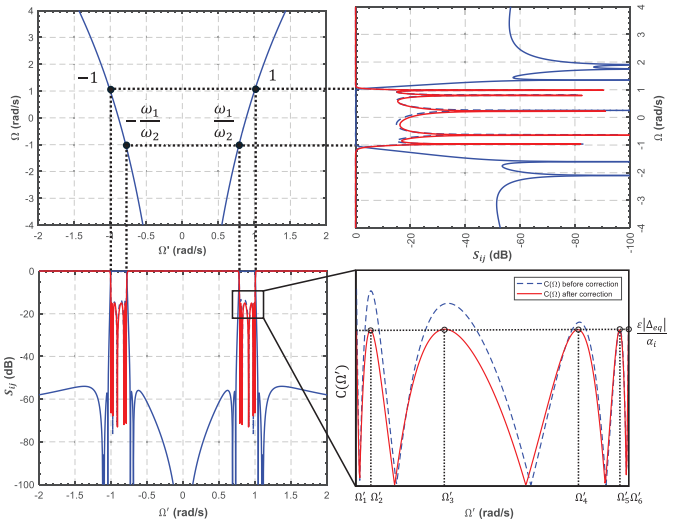

Fig. 5. Mapping an RC function to the dual-band domain using a logarithmic function. The characteristic function $C(\Omega')$ is evaluated between (fc_1/fc_2) and 1 before and after performing the correction with the nonequiripple scaling factors α_i. ε is used to normalize both characteristic functions.

Step 3: As a nonequiripple function, the amplitude Δ_i at each extreme point Ω'_i is different. The equiripple shape can be recovered by modifying those Δ_i using a set of scaling factors α_i. To do this, we will need to choose a reference extreme point, in our case the upper corner of the band where we know that the return loss (RL) level is always the desired one

$$\left|C(\Omega')\right|_{\Omega'=\pm 1} = |\Delta_{eq}|. \tag{4}$$

In this way, we can compute the α_i values that adjust each corresponding Δ_i to be at the same level as Δ_{eq} as follows:

$$\alpha_i = \frac{\Delta_{eq}}{\Delta_i}, \quad i = 1, \ldots, N+1. \tag{5}$$

Step 4: Using the information from α_i, the initial equiripple transfer function $C_{eq}(\Omega)$ in *step 1* can be recalculated and adjusted with (5) to make it nonequiripple as follows:

$$C(\Omega_i) = \alpha_i C_{eq}(\Omega_i). \tag{6}$$

This ensures that after applying the mapping function of (2) again, but now to the nonequiripple response of (6), the resulting mapped function $C_{eq}(\Omega')$ becomes equiripple. Note that the value of α_{N+1} is equal to 1, as it corresponds to the extreme point of the upper corner in (4), where the amplitude Δ_{eq} is already the desired one.

B. Relationship Between the Phase and the I/O Elements

The I/O elements of the DB approach accommodate the mismatch between the reflection phases of the transfer function and the first AW resonator. This phase is frequency-dependent and is managed by conjugate pairs of CRZs. Fig. 6 shows a comparison between the phases corresponding to the LP and DB polynomial magnitude responses of Fig. 4.

Notice how, in the LP approximation, there is a horizontal asymptote approaching 0° as Ω tends to ±∞. According to

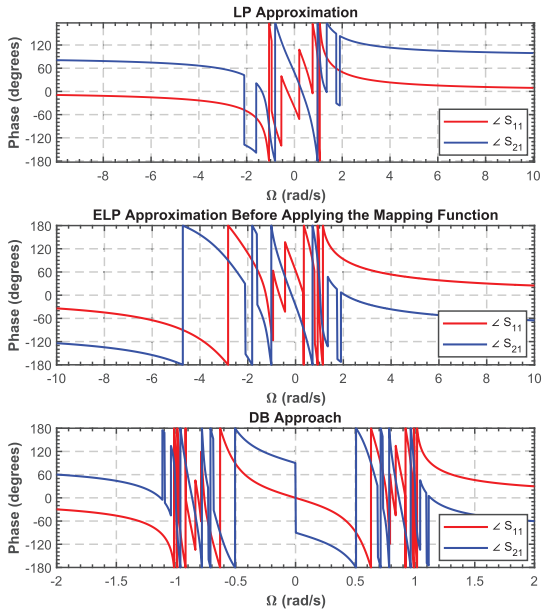

Fig. 6. Transmission and reflection phases corresponding to the LP, ELP, and DB polynomial magnitude responses of Fig. 4.

Amari and Macchiarella [21], this horizontal asymptote is shifted by adding an additional phase term to the reflection phase. Although in the DB approach, the reflection phase also tends to 0° at the vertical asymptotes located at the extreme frequencies, the additional phase term is now interpreted as a pair of conjugate CRZs that control the slope of the reflection phase, rather than shifting the horizontal asymptote up or down. Indeed, these CRZs can be positioned in specific regions where I/O capacitors are not required by equating the following equation to 0° for a shunt-starting or to 180° for a series-starting ladder filter:

$$S_{11}(s) = \left.\frac{F(s)}{E(s)}\right|_{s=\pm j\Omega_{\mathrm{TZ}_1}}. \tag{7}$$

1) Influence of the CRZ When There Are No I/O Inductors: In the DB, there are no I/O inductors when the order of the RC filter function is $N+1$ so that it becomes a $2N+2$ order when it is mapped to the real frequency domain by (2). Thus, a single CRZ is needed to have the same number of in-band RZs as resonators. However, the mapped CRZ (Ω'_{CRZ}) must be purely imaginary for the mapped function to be Hermitian

$$\Omega'_{\mathrm{CRZ}} = 10^{\frac{\Re\{\Omega_{\mathrm{CRZ}}\}-1}{k_U}} \cdot e^{j\frac{\Im\{\Omega_{\mathrm{CRZ}}\}\ln(10)}{k_U}}$$
$$\Omega'_{\mathrm{CRZ}} \in \mathbb{C} : \Re\left\{\Omega'_{\mathrm{CRZ}}\right\} = 0 \tag{8}$$

where k_U is defined in (2). On the other hand, the imaginary part of the CRZ before being mapped (Ω_{CRZ}) must be defined by the following expression:

$$\Im\{\Omega_{\mathrm{CRZ}}\} = \frac{\pi k_U}{2\ln(10)}. \tag{9}$$

The real part of Ω_{CRZ} is a degree of freedom and it manages the I/O capacitors that act as a phase shift, preparing the extraction of the first and last resonators. Therefore, the position of this $\Re\{\Omega_{\mathrm{CRZ}}\}$ has a strong impact not only on

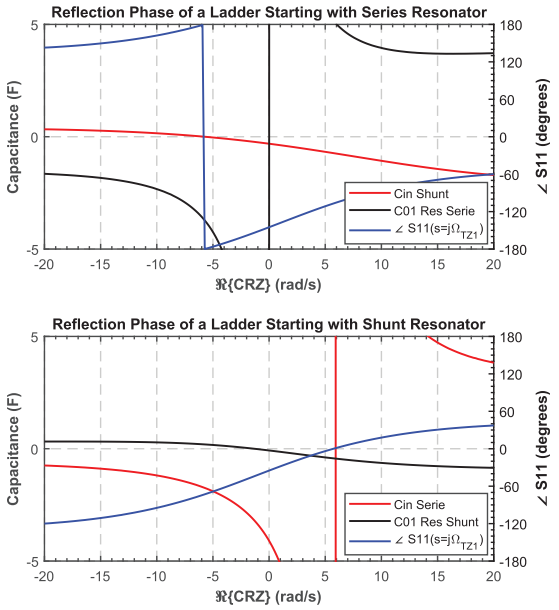

Fig. 7. Sweep of $\Re\{\Omega_{\text{CRZ}}\}$ to compare C_{in} and C_{0_1} against $\angle S_{11}$ evaluated at the first TZ for an AW filter starting with series and shunt resonator.

the value of $C_{\text{I/O}}$ but also on the static capacitance C_0 of all resonators. The $\Re\{\Omega_{\text{CRZ}}\}$ must be positive for series-starting ladder filters and negative for shunt-starting ones to achieve a positive C_0, as it is depicted in Fig. 7. Observe how the position of $\Re\{\Omega_{\text{CRZ}}\}$ that eliminates the I/O capacitors, also corresponds to the point where C_{in} transitions from positive to negative. The position in which $\Re\{\Omega_{\text{CRZ}}\}$ nullifies C_{in} depends on the capacitive contribution of the remaining resonators in the AW ladder filter. When the TZs are close to the passband, the C_0 values typically increase in shunt resonators and decrease in series resonators, leading to a deterioration of the OoB rejection, which is controlled by this capacitance ratio of the ladder topology. In such cases, inductive compensation is required at the beginning and/or end of the AW filter. Since this filtering function does not account for I/O inductors, the inductive compensation appears as negative I/O capacitances, as observed in Fig. 7. For narrowband filters, this behavior is not critical because AW filters can be designed with relatively far-band TZs to improve the OoB rejection while keeping standard AW technologies. This does not happen for wideband filters, since to achieve manufacturing k_t^2, the TZs must be very close to the passband, leading to negative I/O capacitors. In these particular situations, the ladder configuration requires inductive I/O elements to compensate for the negative slopes.

Regarding the magnitude response of the filter, when the presence of I/O capacitors is necessary, they do not significantly affect the OoB rejection (see the black trace in Fig. 8) because the CRZs are located on the imaginary axis. However, if they were omitted, a mismatch would occur, leading to the loss of the filter's equiripple shape. Moreover, their presence can be crucial for accommodating the k_t^2 values of the first and last resonators, as explained in [36].

2) Influence of the CRZ When Considering I/O Inductors: When considering I/O inductors, the order of the DB must be $N+2$ so that it becomes a $2N+4$ order when it is mapped to

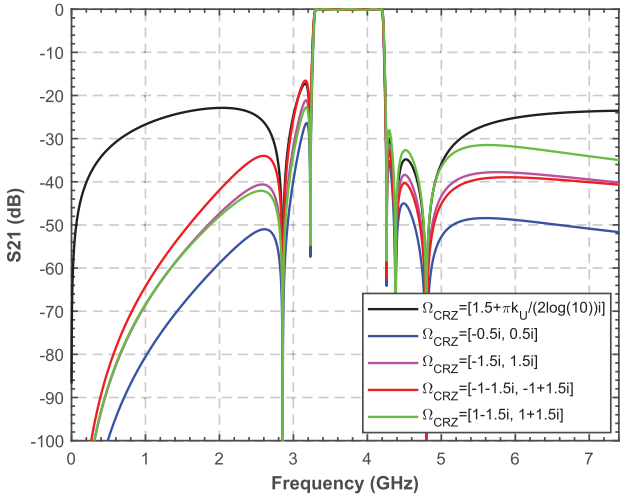

Fig. 8. How the CRZ position influences the OoB rejection in a ladder filter.

the DB domain by (2). In this scenario, the only restriction on the CRZs is that they must be conjugate pairs, ensuring that the resulting dual-band function is Hermitian after mapping. When I/O inductors are included, the CRZs remain linked to the I/O capacitors, and they can be neglected when (7) equals $-90°$ for series-starting resonator and $0°$ for shunt-starting resonator.

Thanks to the inductive contribution of the I/O inductors, both the I/O capacitors and the first and last resonators are usually positive. This allows the TZs to be placed extremely close to the passband while ensuring that all the filter elements remain positive. This increase in the inductive contribution of the filter not only improves the OoB rejection but also reduces the capacitive contribution of the overall network, leading to a lower k_t^2, particularly from the first and last resonators. Therefore, for wideband filters, it is advisable to design them by including these I/O inductors.

In Fig. 8, the magnitude response of a fifth-order series-starting AW filter is compared at OoB frequencies for different CRZ combinations. The possibility of controlling the OoB fly-backs with the CRZs in the DB approach is an additional advantage, since different levels of rejection can be achieved and, consequently, better fulfillment of the passband's far mask specifications. The $\Im\{\Omega_{\text{CRZ}}\}$ controls the overall OoB rejection level, while $\Re\{\Omega_{\text{CRZ}}\}$ regulates the fly-back. As $\Im\{\Omega_{\text{CRZ}}\}$ approaches zero, the I/O inductors become smaller, leading to an improvement in OoB rejection, a decrease in the C_0 of shunt resonators, and an increase in the C_0 of series resonators. However, as the shunt inductor decreases in value, it becomes more sensitive because it stores more energy, being more susceptible to degrading the insertion loss due to its low-quality factor. The opposite occurs as $\Im\{\Omega_{\text{CRZ}}\}$ moves away from zero. Let us highlight that $\Re\{\Omega_{\text{CRZ}}\}$ must remain significantly lower than $\Im\{\Omega_{\text{CRZ}}\}$ to prevent excessive fly-back levels and impractical k_t^2.

C. Improving Accuracy in Defining the DB Filtering Function

In general, numerical errors can significantly impact the computation of Feldtkeller's equation in the bandpass domain,

as high-order polynomials generate large coefficients that exceed double floating-point precision when the network order is greater than 5 (i.e., a 12th-order DB filter) or when the FBW is below 10%. To address this limitation, the roots of $P(s)$ and $F(s)$, namely $\{zP = j\Omega'_{\mathrm{TZ}}\}$ and $\{zF = j\Omega'_{\mathrm{RZ}}\}$, respectively, which are already available once the RC filtering function is mapped using (2), are utilized to directly compute the ratio between the normalization constants $\varepsilon/\varepsilon_r$ by evaluating the following expression at $s = \pm j$:

$$\frac{\varepsilon}{\varepsilon_r} = \frac{1}{\sqrt{10^{RL/10}-1}}\left|\frac{P(s)}{F(s)}\right| \tag{10}$$

where

$$P(s) = \prod_{i=1}^{N_{\mathrm{TZ}}}(j - zP_i); \quad F(s) = \prod_{m=1}^{N_{\mathrm{DB}}}(j - zF_m). \tag{11}$$

To recalculate the polynomial $E(s)$, it is possible to use the iterative computational method described in [23], which introduces an arbitrary common denominator $Q(s)Q(s)^*$ to both sides of the Feldtkeller equation to improve the accuracy of solutions up to order 39. However, this method is designed for the LP approximation, since the passband is defined in $\Omega = [-1, 1]$, rather than $\Omega' = [-1, -fc_1/fc_2; fc_1/fc_2, 1]$, as in the DB approach. In this situation, the roots are extremely clustered, which makes this method fail even for low orders due to its dependence on coefficients. This issue can be solved by adapting the iterative procedure in [23] to work with roots. In fact, this root-based methodology will also be used during the parameter extraction in Section III-A. First, let us define the Feldtkeller equation with the common denominator as follows:

$$\frac{E(s)E(s)^*}{Q(s)Q(s)^*} = \frac{P(s)P(s)^*}{Q(s)Q(s)^*} + \frac{F(s)F(s)^*}{Q(s)Q(s)^*} \tag{12}$$

where the roots $\{zQ\}$ of $Q(s)$ must be defined in the first iteration of the iterative procedure as the mapped roots $\{zE\}$ of $E(s)$, using the logarithmic mapping function of (2) to accelerate the convergence process to 2 or 3 iterations, regardless of filter order and bandwidth. Although the mapped zE are incorrect, they are already very close to the desired zE

$$zQ^{(0)} = zE. \tag{13}$$

Knowing zQ, the partial fraction expansions of both terms on the right-hand side of (12) can be calculated as follows:

$$\frac{P(s)P(s)^*}{Q(s)Q(s)^*} = |K_P|^2 + \sum_k^{N_{\mathrm{DB}}}\left(\frac{c_{k,P}}{s-p_k} - \frac{c^*_{k,P}}{s+p^*_k}\right) \tag{14}$$

$$\frac{F(s)F(s)^*}{Q(s)Q(s)^*} = |K_F|^2 + \sum_k^{N_{\mathrm{DB}}}\left(\frac{c_{k,F}}{s-p_k} - \frac{c^*_{k,F}}{s+p^*_k}\right). \tag{15}$$

The operation of both partial fraction expansions must be expressed in terms of the roots of their numerators and denominators. The poles p_k correspond directly to the roots zQ of the denominator $Q(s)$, the constant term K_F is set to 1 because the evaluated polynomials are always monic, and the constant term K_P is set to 0 because the numerator's order is always lower than the denominator's. Regarding to the residues $c_{k,P}$ and $c_{k,F}$, they are defined as follows:

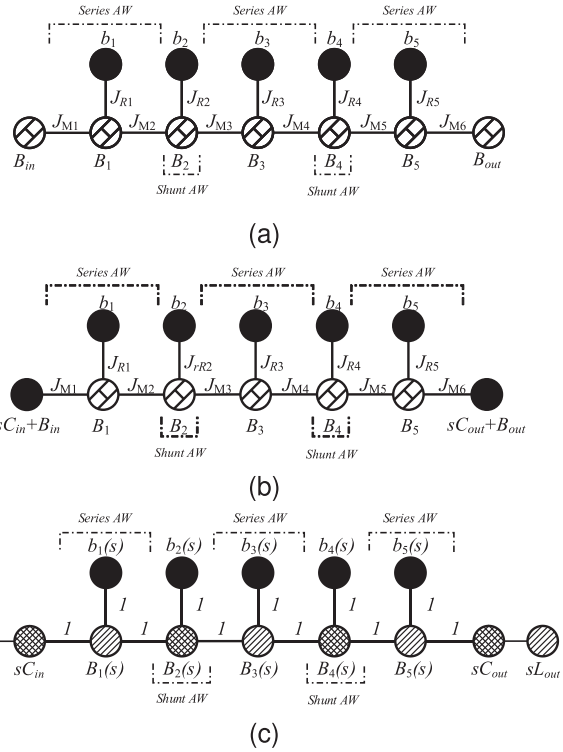

Fig. 9. Nodal representation of a fifth-order ladder network starting in series AW resonator depending on each technique. (a) LP, (b) ELP, and (c) DB.

$$c_{k,P} = \frac{\prod_{i=1}^{N_{\mathrm{TZ}}}(p_k - zP_i)}{\prod_{m=1,m\neq k}^{N_{\mathrm{DB}}}(p_k - zQ_m)} \cdot \frac{\prod_{i=1}^{N_{\mathrm{TZ}}}\left(p_k - zP^*_i\right)}{\prod_{m=1}^{N_{\mathrm{DB}}}\left(p_k - zQ^*_m\right)} \tag{16}$$

$$c_{k,F} = \frac{\prod_{m=1}^{N_{\mathrm{DB}}}(p_k - zF_m)}{\prod_{m=1,m\neq k}^{N_{\mathrm{DB}}}(p_k - zQ_m)} \cdot \frac{\prod_{m=1}^{N_{\mathrm{DB}}}\left(p_k - zF^*_m\right)}{\prod_{m=1}^{N_{\mathrm{DB}}}\left(p_k - zQ^*_m\right)}. \tag{17}$$

Then, the residues and constant terms corresponding to the left-hand side of (12) can be calculated as follows:

$$\frac{E(s)E(s)^*}{Q(s)Q(s)^*} = |K|^2 + \sum_k^{N_{\mathrm{DB}}}\left(\frac{r_k}{s-p_k} - \frac{r^*_k}{s+p^*_k}\right) \tag{18}$$

where

$$|K|^2 = |K_P|^2 + |K_F|^2; \quad r_k = c_{k,P} + c_{k,F}. \tag{19}$$

Once the partial fraction expansion is determined, the new roots $zQ^{(v+1)}$ are recalculated as the eigenvalues of the matrix $(\mathbf{A} - \mathbf{B}d^{-1}\mathbf{C}^T)$, applying the iterative pole relocation strategy until obtaining zE after convergence, as described in [23].

III. Synthesis and Parameter Extraction

AW ladder filters, such as the networks depicted in Fig. 2(a) and (b), have different nodal representations depending on whether the LP, ELP, or DB model is used, as shown in Fig. 9(a)–(c), respectively. The LP and ELP approximations are composed of N dangling resonator sections made of resonant nodes (a unitary capacitor in parallel with an FIR b) connected to nonresonant nodes (an FIR B) via admittance

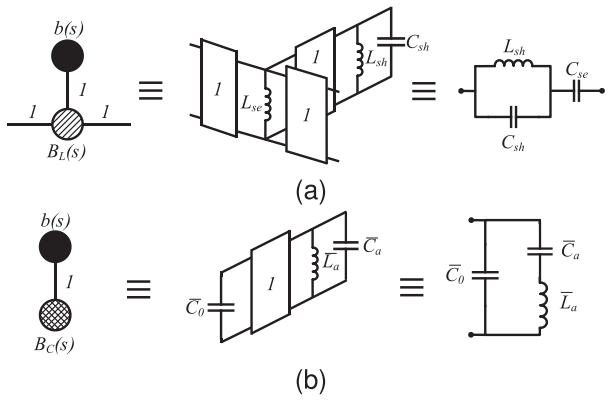

Fig. 10. Nodal representation, equivalent circuit, and BVD model of the DB-extracted pole section in Fig. 9(c). (a) Series resonator and (b) shunt resonator.

inverters J_R. The input admittance of each extracted pole section is defined as follows:

$$Y_{\mathrm{EP}}(s) = jB_i + \frac{J_R^2}{s + jb_i}. \tag{20}$$

These admittance characteristics show a direct relationship with normalized BVD models, as explained in [4]. In addition, I/O FIRs arranged in shunt are usually scaled as inductors when their sign is negative and as capacitors when their sign is positive, and vice versa for series-connected FIRs, since the sign is directly related to the FIR input phase. Note that the ELP uses resonant nodes as I/O elements instead of nonresonant nodes to improve the modeling of asymptotes at infinity. However, ELP cannot model TZs at zero because the remaining FIRs prevent any contribution at the origin, making this approximation still imperfect, especially when the finite TZs are very close to the passband.

The proposed DB approach is also composed of N extracted pole sections where now, there are more frequency-dependent nodes than the LP and ELP to model the remaining asymptotes at origin and infinity. Resonant nodes are represented by a shunt capacitor in parallel with a shunt inductor and nonresonant nodes are replaced by reactance nodes [37] composed by shunt capacitors or shunt inductors to represent a series or a shunt resonator, respectively. As it is depicted in Fig. 10(a) and (b), both extracted pole sections are directly related to the normalized bandpass BVD model, as they provide an exact representation of it. This occurs because all inverters are unitary, and the main-line inverters maintain a consistent sign due to the inherent alternation between extracted pole admittance functions. Consequently, the unitary main-line inverters cause the inductor L_{se} to change in nature in series resonators, becoming a capacitor C_{se}, as shown in Fig. 10(a). Thus, the input admittance of each extracted pole section, depending on whether it represents a series or a shunt resonator, is defined as follows:

$$\begin{aligned} Y_{\mathrm{EP_{SHU}}}(s) &= s\bar{C}_0 + \frac{1}{s\bar{L}_a + \frac{1}{s\bar{C}_a}} \\ Y_{\mathrm{EP_{SER}}}(s) &= \frac{1}{s\bar{L}_{se}} + \frac{1}{s\bar{L}_{sh} + \frac{1}{s\bar{C}_{sh}}} \end{aligned} \tag{21}$$

where the superscript $\bar{}$ denotes the normalized form of an element. Each extracted pole section contributes with two TZs when the impedance of the series branch is minimum

$$s\bar{L}_a + \frac{1}{s\bar{C}_a} = 0 \rightarrow s = \pm\frac{j}{\sqrt{\bar{L}_a\bar{C}_a}} \tag{22}$$

which coincide with the normalized BVD series frequency f_s. In addition, it also contributes with two attenuation poles when the total admittance is minimum

$$s\bar{C}_0 + \frac{1}{s\bar{L}_a + \frac{1}{s\bar{C}_a}} = 0 \rightarrow s = \pm j\sqrt{\frac{\bar{C}_a + \bar{C}_0}{\bar{L}_a\bar{C}_a\bar{C}_0}} \tag{23}$$

which coincides with the normalized BVD parallel frequency f_p. The set of characteristic polynomials defined in (1) are transformed into the normalized circuit elements that implement the ladder topology using the extracted pole method [21], [38], which is based on sequentially extracting circuit elements from a global admittance function, defined as follows:

$$Y_{\mathrm{in}}(s) = \frac{E(s) - F(s)}{E(s) + F(s)}. \tag{24}$$

To perform the parameter extraction, the input admittance associated with the characteristic polynomials in (24) must be set equal to that of the network being analyzed as follows:

$$Y_{\mathrm{in}}(s) = \frac{1}{s\bar{L}_{\mathrm{in}}} + s\bar{C}_{\mathrm{in}} + \cfrac{1}{y_{\mathrm{EP}_1}(s) + \ldots + \cfrac{1}{y_{\mathrm{EP}_N}(s) + \cfrac{1}{\cfrac{1}{s\bar{L}_{\mathrm{out}}} + s\bar{C}_{\mathrm{out}} + G_L}}}. \tag{25}$$

Once the admittance parameters are obtained, the values of the circuit elements in the network can be determined through partial or complete extraction of residues at each TZ.

A. Improving Accuracy During the Parameter Extraction

The extracted pole technique for high-order filters is traditionally hampered by numerical rounding errors that accumulate at each step [21], [22], something that is very critical in a DB methodology whose characteristic polynomials double the order of the LP. Following the same root-based philosophy described in Section II-C, the admittance function can be updated without losing accuracy. Instead of using (13) as the initial seed $zQ^{(0)}$ to determine the roots of (24), now $zQ^{(0)}$ is calculated as the roots of the numerator and denominator admittance functions of (24) using the MATLAB's *roots* function. First, the numerator and the denominator of the right-hand side of (24) must be redefined as follows:

$$\frac{E(s)}{Qn(s)} - \frac{F(s)}{Qn(s)} = \frac{1}{\varepsilon_n}\sum_{k}^{N_{\mathrm{DB}}}\left(\frac{r_{k,E}}{s - p_k} - \frac{r_{k,F}}{s - p_k}\right) \tag{26}$$

$$\frac{E(s)}{Qd(s)} + \frac{F(s)}{Qd(s)} = \frac{1}{\varepsilon_d}\sum_{k}^{N_{\mathrm{DB}}}\left(\frac{r_{k,E}}{s - p_k} + \frac{r_{k,F}}{s - p_k}\right) \tag{27}$$

where $\varepsilon_n = E_2(s) - F_2(s)$ and $\varepsilon_d = E_1(s) + F_1(s)$ are the numerator and denominator denormalization constants that keep information about the higher-order polynomial coefficients during the iterative procedure, and the residues $r_{k,E}$ and $r_{k,F}$ are defined as follows:

$$r_{k,E} = \frac{\prod_{m=1}^{N_{\mathrm{DB}}}(p_k - zE_m)}{\prod_{m=1,m\neq k}^{N_{\mathrm{DB}}}(p_k - zQ_m)};\quad r_{k,F} = \frac{\prod_{m=1}^{N_{\mathrm{DB}}}(p_k - zF_m)}{\prod_{m=1,m\neq k}^{N_{\mathrm{DB}}}(p_k - zQ_m)}. \tag{28}$$

TABLE II

HOW TO MODIFY THE REFERENCE EXPRESSIONS (29) AND (30) FOR UPDATING THE ADMITTANCE FUNCTION AFTER EACH ELEMENT EXTRACTION

Update the numerator of expression	$zY1$	$zY2$	ε_3	ε_1	ε_2	Initial Seed ($zQ^{(0)}$) of the iterative procedure
(32)	$s \cdot zYd$	zYn	ε_n	$\varepsilon_d \bar{L}_{in}$	ε_n	*roots* of $\left(\frac{1}{Y_{in}(s)} - \frac{1}{s\bar{L}_{in}}\right)$
(35)	$s \cdot zYd$	zYn	$\varepsilon_d \bar{C}_{in} - \varepsilon_n$	$\varepsilon_d \bar{C}_{in}$	ε_n	*roots* of $\left(\frac{1}{Y_{in}(s)} - \frac{1}{s\bar{C}_{in}}\right)$
(37)	zYd	$s \cdot zYn$	$\varepsilon_d - \varepsilon_n \bar{C}_{in}$	ε_d	$\varepsilon_n \bar{C}_{in}$	*roots* of $\left(\frac{1}{Y_{in}(s)} - s\bar{C}_{in}\right)$
(40)	$(s^2 + \Omega^2_{TZ_n}) \cdot zYn$	$s \cdot zYd$	$\varepsilon_n - \varepsilon_d / \bar{C}_{sh}$	ε_n	$\varepsilon_d / \bar{C}_{sh}$	*roots* of $\left(Y_{in}(s) - \frac{s/\bar{C}_{sh}}{(s^2+\Omega^2_{TZ_n})}\right)$
(42)	$s \cdot zYn$	zYd	$\varepsilon_n \bar{C}_{se} - \varepsilon_d$	$\varepsilon_n \bar{C}_{se}$	ε_d	*roots* of $\left(Y_{in}(s) - \frac{1}{s\bar{C}_{se}}\right)$
(46)	$(s^2 + \Omega^2_{TZ_n}) \cdot zYd$	$s \cdot zYn$	ε_d	ε_d	$\varepsilon_n / \bar{L}_a$	*roots* of $\left(\frac{1}{y_{in}(s)} - \frac{s/\bar{L}_a}{(s^2+\Omega^2_{TZ_n})}\right)$
(48)	zYd	$s \cdot zYn$	$\varepsilon_d - \varepsilon_n \bar{C}_0$	ε_d	$\varepsilon_n \bar{C}_0$	*roots* of $\left(\frac{1}{y_{in}(s)} - s\bar{C}_0\right)$

Once both iterative procedures converge after the $(v+1)$ iterations, $\{zYn\} = zQn^{(v+1)}$ will represent the precise roots of the numerator of (24), while $\{zYd\} = zQd^{(v+1)}$ will correspond to the roots of its denominator.

Regarding parameter extraction, the procedure is quite similar. Each time an element is extracted, the admittance function must be updated by subtracting the extracted element from the current admittance to obtain the precise updated roots zYn or zYd. This process can be generalized for all admittance updates by expressing them into two terms as follows:

$$\frac{Y1(s)}{Q(s)} + \frac{Y2(s)}{Q(s)} = \frac{1}{\varepsilon_3} \sum_{k}^{N_Q} \left(\varepsilon_1 \frac{r_k^{(1)}}{s - p_k} + \varepsilon_2 \frac{r_k^{(2)}}{s - p_k} \right) \tag{29}$$

where N_Q is the number of roots of the initial seed $zQ^{(0)}$ after each element extraction, and residues $r_k^{(1)}$ and $r_k^{(2)}$ are

$$r_k^{(1)} = \frac{\prod_{m=1}^{N_{zY1}} (p_k - zY1_m)}{\prod_{m=1, m\neq k}^{N_Q} (p_k - zQ_m)};\ r_k^{(2)} = \frac{\prod_{i=1}^{N_{zY2}} (p_k - zY2_m)}{\prod_{m=1, m\neq k}^{N_Q} (p_k - zQ_m)}. \tag{30}$$

Using expressions (29) and (30) as a reference, Table II aims to summarize how to update the admittance function after each parameter extraction, where ε_1, ε_2 and ε_3 are the coefficients necessary to restore the scale of the polynomial. Note that Table II defines the updates to the numerators of expressions (32), (35), (37), (40), (42), (46), and (48) rather than to the admittance functions themselves. Indeed, their denominators do not need an iterative procedure to be updated. In addition, multiplying the current zYn or zYd by s is equivalent to adding an extra root at the origin, while multiplying by $(s^2 + \Omega^2_{\mathrm{TZ}_n})$ corresponds to adding two additional roots at $\pm\Omega_{\mathrm{TZ}_n}$.

1) Extraction of I/O Elements: If the transfer function is designed to include I/O inductors, a shunt-connected inductor is extracted through a partial extraction, with its corresponding residue exhibiting a single pole at the origin

$$\bar{L}_{\mathrm{in}} = \left. \frac{\varepsilon_d \cdot zYd}{\varepsilon_n \cdot s \cdot zYn} \right|_{s=0} \tag{31}$$

$$\frac{zYd}{zYn} \leftarrow \frac{zYd \cdot s\bar{L}_{\mathrm{in}} - zYn}{zYn \cdot s\bar{L}_{\mathrm{in}}};\ \frac{\varepsilon_d}{\varepsilon_n} \leftarrow \frac{\varepsilon_d \bar{L}_{\mathrm{in}} - \varepsilon_n}{\varepsilon_n \bar{L}_{\mathrm{in}}}. \tag{32}$$

After updating the numerator in (32), remove the two roots at the origin that are canceled out due to their presence in both the numerator and the denominator.

When the first resonator is placed in shunt, the reactance function must be inverted because the connection and the introduced TZ value by the capacitor are different

$$\frac{zYn}{zYd} \leftarrow \frac{zYd}{zYn}. \tag{33}$$

Then, the input series-connected capacitor is evaluated at the first TZ and it also contributes in TZ at the origin

$$\bar{C}_{\mathrm{in}} = \frac{\varepsilon_n \prod_{m=1}^{N_{zYn}} (j\Omega_{\mathrm{TZ}_1} - zYn_m)}{\varepsilon_d \prod_{m=1}^{N_{zYd}} (j\Omega_{\mathrm{TZ}_1} - s \cdot zYd_m)} \tag{34}$$

$$\frac{zYn}{zYd} \leftarrow \frac{zYd \cdot s\bar{C}_{\mathrm{in}} - zYn}{zYn \cdot s\bar{C}_{\mathrm{in}}};\quad \frac{\varepsilon_n}{\varepsilon_d} \leftarrow \frac{\varepsilon_d \bar{C}_{\mathrm{in}} - \varepsilon_n}{\varepsilon_n}. \tag{35}$$

On the other hand, when the first resonator is placed in series, the input shunt-connected capacitor is evaluated at the first TZ and it also contributes in TZ at infinity

$$\bar{C}_{\mathrm{in}} = \frac{\varepsilon_d \prod_{m=1}^{N_{zYd}} (j\Omega_{\mathrm{TZ}_1} - zYd_m)}{\varepsilon_n \prod_{m=1}^{N_{zYn}} (j\Omega_{\mathrm{TZ}_1} - s \cdot zYn_m)} \tag{36}$$

$$\frac{zYd}{zYn} \leftarrow \frac{zYd - zYn \cdot s\bar{C}_{\mathrm{in}}}{zYn};\quad \frac{\varepsilon_d}{\varepsilon_n} \leftarrow \frac{\varepsilon_d - \bar{C}_{\mathrm{in}}\varepsilon_n}{\varepsilon_n}. \tag{37}$$

2) Extraction of Series and Shunt AW Resonators: AW series resonators, like the one shown in Fig. 10(a), prepare for the annihilation of the next TZ from the subsequent shunt resonator and it also contributes to the TZ at the origin. To extract an AW series resonator, the values of capacitor $\bar{C}_{\mathrm{sh}}$ and inductor $\bar{L}_{\mathrm{sh}}$ are calculated as follows:

$$\bar{C}_{sh} = \left. \frac{\varepsilon_d \cdot \prod_{m=1}^{N_{zYd}} (s - s \cdot zYd_m)}{2\varepsilon_n \cdot (s^2 + \Omega^2_{\mathrm{TZ}_n}) \prod_{m=1}^{N_{zYn}} (s - zYn_m)} \right|_{s=\pm j\Omega_{\mathrm{TZ}_n}} \tag{38}$$

$$\bar{L}_{sh} = \frac{1}{\Omega^2_{\mathrm{TZ}_n} \bar{C}_{sh}} \tag{39}$$

$$\frac{zYn}{zYd} \leftarrow \frac{zYn(s^2 + \Omega^2_{\mathrm{TZ}_n}) - zYd \cdot s/\bar{C}_{sh}}{zYd \cdot (s^2 + \Omega^2_{\mathrm{TZ}_n})}$$

$$\frac{\varepsilon_n}{\varepsilon_d} \leftarrow \frac{\varepsilon_n - \varepsilon_d/\bar{C}_{sh}}{\varepsilon_d}. \tag{40}$$

Note that the term $(s^2 + \Omega^2_{\mathrm{TZ}_n})$ indicates that these roots are removed from those of zYd, and the coefficient 2 arises from the multiplicity of the pole. After obtaining the elements of an extracted poled section, the numerator's order increases by 2 due to the addition of the TZs, which must be removed from

both the numerator and denominator after updating. Then, capacitor C_{se} must be computed as follows:

$$\bar{C}_{se} = \frac{\varepsilon_d \prod_{m=1}^{N_{zYd}} (j\Omega_{\mathrm{TZ}_{n+1}} - zYd_m)}{\varepsilon_n \prod_{m=1}^{N_{zYn}} (j\Omega_{\mathrm{TZ}_{n+1}} - s \cdot zYn_m)} \tag{41}$$

$$\frac{zYn}{zYd} \leftarrow \frac{zYn \cdot s\bar{C}_{se} - zYd}{zYd \cdot s\bar{C}_{se}}; \quad \frac{\varepsilon_n}{\varepsilon_d} \leftarrow \frac{\varepsilon_n \bar{C}_{se} - \varepsilon_d}{\varepsilon_d \bar{C}_{se}}. \tag{42}$$

Finally, a Star-to-Delta transformation must be performed to obtain the desired normalized BVD elements

$$\bar{C}_0 = \frac{\bar{C}_{se}}{1 + \bar{C}_{se}/\bar{C}_{sh}}; \quad \bar{C}_a = \frac{\bar{C}_{se}}{1 + \bar{C}_{sh}/\bar{C}_{se}}$$
$$\bar{L}_a = \bar{L}_{sh} \left(\frac{\bar{C}_{sh} + \bar{C}_{se}}{\bar{C}_{se}} \right)^2. \tag{43}$$

In contrast, AW shunt resonators, like the one shown in Fig. 10(b), prepare for the annihilation of the next TZ from the subsequent series resonator and it also contributes to the TZ at infinity. To extract an AW shunt resonator, inductor $\bar{L}_a$ and capacitor $\bar{C}_a$ must be computed as follows:

$$\bar{L}_a = \left. \frac{\varepsilon_n \cdot \prod_{m=1}^{N_{zYn}} (s - zYn_m)}{2\varepsilon_d \cdot (s^2 + \Omega_{\mathrm{TZ}_n}^2) \prod_{m=1}^{N_{zYd}} (s - zYd_m)} \right|_{s=\pm j\Omega_{\mathrm{TZ}_n}} \tag{44}$$

$$\bar{C}_a = \frac{1}{\Omega_{\mathrm{TZ}_n}^2 \bar{L}_a} \tag{45}$$

$$\frac{zYd}{zYn} \leftarrow \frac{zYd\left(s^2 + \Omega_{\mathrm{TZ}_n}^2\right) - \frac{s \cdot zYn}{\bar{L}_a}}{zYn\left(s^2 + \Omega_{\mathrm{TZ}_n}^2\right)}; \quad \frac{\varepsilon_d}{\varepsilon_n} \leftarrow \frac{\varepsilon_d}{\varepsilon_n} \tag{46}$$

where ε_n and ε_d remain the same because the order of the denominator is much greater than that of the numerator. Finally, capacitor C_0 is defined as follows:

$$\bar{C}_0 = \frac{\varepsilon_d \prod_{m=1}^{N_{zYd}} (j\Omega_{\mathrm{TZ}_{n+1}} - zYd_m)}{\varepsilon_n \prod_{m=1}^{N_{zYn}} (j\Omega_{\mathrm{TZ}_{n+1}} - s \cdot zYn_m)} \tag{47}$$

$$\frac{zYd}{zYn} \leftarrow \frac{zYd - s\bar{C}_0 \cdot zYn}{zYn}; \quad \frac{\varepsilon_d}{\varepsilon_n} \leftarrow \frac{\varepsilon_d - \varepsilon_n C_0}{\varepsilon_n}. \tag{48}$$

3) Last Extraction: During the last extraction, there is no need to still use the previous root-based methodology, as the remaining admittance polynomials are properly handled with coefficients. If the last resonator is placed in series, the last elements should be calculated as follows:

$$\bar{C}_{se} = y_{\mathrm{in}}(s)\Big|_{s=0} \tag{49}$$

$$y_{\mathrm{in}}(s) \leftarrow y_{\mathrm{in}}(s) - \frac{1}{s\bar{C}_{se}} \tag{50}$$

$$y_{\mathrm{in}}(s) = \frac{1}{sL_{\mathrm{out}}} + s\bar{C}_{\mathrm{out}} + \frac{1}{G_L} \tag{51}$$

while if it is placed in a shunt as follows:

$$\bar{C}_0 = \left. \frac{1}{s y_{\mathrm{in}}(s)} \right|_{s=\infty} \tag{52}$$

$$y_{\mathrm{in}}(s) \leftarrow y_{\mathrm{in}}(s) - s\bar{C}_0 \tag{53}$$

$$y_{\mathrm{in}}(s) = \frac{1}{s\bar{C}_{\mathrm{out}}} + y_{rem}(s) \tag{54}$$

$$y_{\mathrm{in}}(s) \leftarrow y_{\mathrm{in}}(s) - \frac{1}{s\bar{C}_{\mathrm{out}}} \tag{55}$$

$$y_{\mathrm{in}}(s) = \frac{1}{s\bar{L}_{\mathrm{out}}} + G_L. \tag{56}$$

Ideally, the admittance function should be equal to 1 when extracting the last frequency-dependent element to achieve a 50-Ω terminated filter. However, in the case of asymmetric networks, a mismatch is typically observed between the topology and the transfer function to be implemented, causing the load conductance (G_L) after extracting the last element to be different from 1.

B. Frequency Transformation

The DB extracted elements are denormalized with a lowpass-to-lowpass frequency transformation [12] because a dual-band symmetric about 0 already exists

$$\Omega = \frac{\omega}{\omega_2}. \tag{57}$$

Therefore, the capacitors and inductors that conform to the BVD model of each resonator still have the same nature when scaling them

$$C_0 = \frac{\bar{C}_0}{Z_0\omega_2}; \qquad C_a = \frac{\bar{C}_a}{Z_0\omega_2}; \qquad L_a = \frac{\bar{L}_a Z_0}{\omega_2}. \tag{58}$$

In the same way, the I/O elements are scaled as follows:

$$L_{I/O} = \frac{\bar{L}_{I/O} Z_0}{\omega_2}; \qquad C_{I/O} = \frac{\bar{C}_{I/O}}{Z_0\omega_2}. \tag{59}$$

IV. Synthesis Validation

In this section, two examples are presented: an eighth-order filter to illustrate the proposed methodology, and a 38th-order filter to verify numerical stability. Note that, in practice, these examples correspond to a third-order and an 18th-order AW ladder filter, respectively, where the order N reflects the number of AW resonators rather than the order N_{DB} of the transfer function.

A. Third-Order AW Ladder Filter

To demonstrate the validity of the DB methodology, this example presents the complete synthesis procedure to obtain the same third-order wideband AW ladder filter starting in the shunt resonator of [24]. This thin-film lithium niobate AW filter operates from 21.35 to 25.65 GHz, that is, an FBW of 18.2%. I/O inductors are not taken into account and the following normalized TZ and CRZ configuration has been chosen: $\Omega_{\mathrm{TZ}} = [-1.707, 1.928, -1.707]$ and $\Omega_{\mathrm{CRZ}} = -10.00 + 17.12i$ designed for a RL = 12 dB. Note that $\Im\{\Omega_{\mathrm{CRZ}}\}$ is fixed by (9) to ensure symmetry with respect to the origin after the frequency mapping. The characteristic polynomials of the RC function are determined as described in [33], resulting in the following polynomial coefficients:

$$P(s) = [1.000, 1.486i, 3.669, 5.619i]$$
$$F(s) = [1.000, 17.121 + 10.357i, -2.808 + 6.113i, 13.050 + 7.829i, -2.070 + 3.545i]$$
$$E(s) = [1.000, 19.029 + 10.357i, 21.668 + 21.365i, 27.935 + 26.490i, 7.677 + 24.282i].$$

To obtain the DB filtering function, the logarithmic mapping function described in (2) is used to construct a dual-band

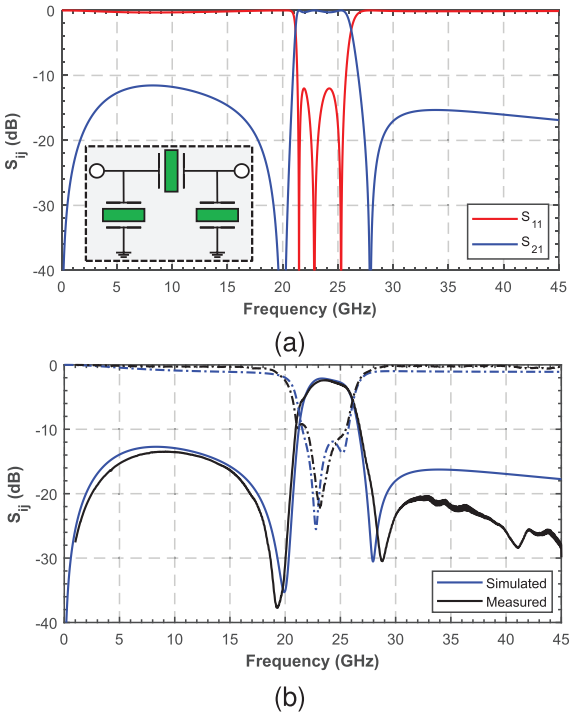

Fig. 11. Third-order AW ladder of the milter operating from 21.35 to 25.65 GHz. (a) Synthesized response using the proposed DB methodology and (b) comparison between its lossy model (blue trace) and the measured fabricated filter (black trace).

TABLE III

BVD ELEMENTS OF THE SYNTHESIZED THIRD-ORDER WIDEBAND AW FILTER EXTRACTED USING THE PROPOSED DB METHODOLOGY

Resonator	L_a (nH)	C_a (fF)	C_0 (fF)	k_t^2 (%)
1 (SH)	0.938	67.460	189.149	44
2 (SE)	1.993	21.977	63.053	43
3 (SH)	0.938	67.460	189.149	44
C_{in} (pF)	No		C_{out} (pF)	No
Z_S (Ω)	50		Z_L (Ω)	50

located at $\Omega' = [-1, -21.35/25.65; 21.35/25.65, 1]$. Then, the set of scaling factors that recover the equiripple response is calculated with (5), resulting in

$$\alpha = [1.079, 1.068, 1.026, 1.000]\,.$$

After recalculating the RC polynomials including this set of scaling factors, the new dual-band mapped roots are computed using (2), leading to

$$\Omega'_{\text{TZ}} = [0.780, -0.780, 1.089, -1.089, 0.780, -0.780, 0]$$
$$\Omega'_{\text{RZ}} = [0.364i, 0.364i, 0.986, -0.986, 0.837. - 0.837$$
$$0.892, -0.892]\,.$$

Then, the elements that compose the ladder network defined with the DB approach are extracted as explained in Section III and listed in Table III, resulting in the filter response shown in Fig. 11(a). Assuming the same mBVD model from [24], but using the extracted parameters of Table III, Fig. 11(b) compares the DB-simulated response with the measured fabricated filter, demonstrating very good agreement, not only in the response, but also with the resulting manufactured parameters in [24]. The parasitic effects of the layout are not considered in the simulated filter, which explains those small discrepancies between both responses. Note that, as explained in Section II-B, this example does not include I/O capacitors because the CRZ has been placed such that $\angle S_{11}(s)|_{\pm j\Omega_{\text{TZ}_1}} = 0°$, nullifying them in both the simulated and fabricated filters. Let us highlight that AW ladder filters require a k_t^2 of approximately twice their FBW [39], which imposes a technological limitation for filters with an FBW greater than 3.5% when using standard technologies, such as standard AlN, which performs with $k_t^2 = 6.7\%$. To design the wideband filter of Fig. 11(b) with an FBW of 18.2%, it was necessary to use resonators with k_t^2 values of 44% and 45%, which aligns with this rule of thumb.

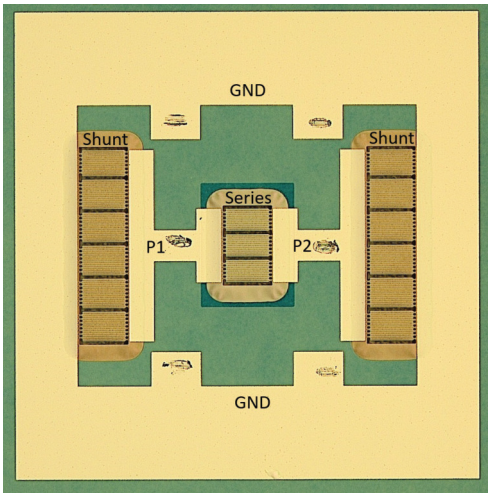

Fig. 12. Microscopic image of the fabricated third-order AW ladder filter starting with the shunt resonator.

The optical image of this fabricated standalone AW ladder filter is depicted in Fig. 12, which has a small footprint of 0.75 × 0.74 mm. The resonators consist of an array of interdigitated transducers (IDTs) placed on top of a 128° Y-cut $LiNbO_3$ thin film with a thickness of 158 nm. The piezoelectric material is suspended over a silicon (Si) substrate with a 1-μm-thick amorphous silicon (a-Si) bounding layer and the electrodes of the IDTs are made of aluminum (Al). The resonance frequency of the shunt and series resonators is fine-tuned by reducing the $LiNbO_3$ layer thickness to 90 and 70 nm, respectively, by using ion beam-assisted argon gas cluster trimming.

B. 18th-Order AW Ladder Filter

To validate the numerical stability of the proposed DB methodology, a hypothetical narrowband 18th-order AW ladder filter operating between 1805 and 1880 MHz (FBW = 4%) has been synthesized. The chosen configuration includes the following normalized TZs and CRZs: $\Omega_{\text{TZ}} = [1.6, -1.5, 1.2, -1.12, 1.1, -1.2, 1.18, -1.5, \quad 1.14, -1.5, 1.18, -1.2, 1.1, -1.12, 1.2, -1.5, 1.6, -1.09]$ and $\Omega_{\text{CRZ}} = 6.9 + 77.17i$ designed for an RL = 12 dB. The resulting extracted elements are listed in Table IV, while the filter response is depicted

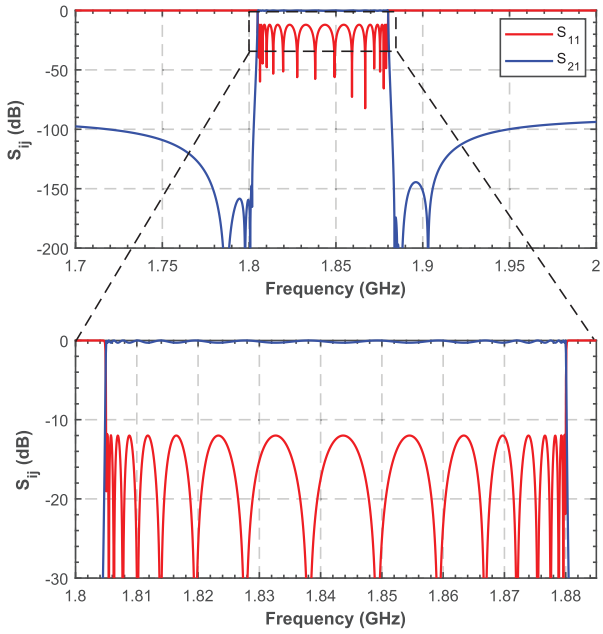

Fig. 13. Response of a hypothetical narrowband 18th-order AW ladder filter synthesized to validate numerical stability.

TABLE IV

BVD ELEMENTS OF THE SYNTHESIZED 18TH-ORDER NARROWBAND AW FILTER EXTRACTED USING THE PROPOSED DB METHODOLOGY

Resonator	L_a (nH)	C_a (fF)	C_0 (pF)	Resonator	L_a (nH)	C_a (fF)	C_0 (pF)
1 (SE)	58.745	129.390	1.490	10 (SH)	39.395	201.414	2.731
2 (SH)	51.368	154.467	2.651	11 (SE)	160.314	46.313	1.062
3 (SE)	136.372	54.590	1.155	12 (SH)	80.833	96.969	1.795
4 (SH)	120.691	64.734	1.476	13 (SE)	120.482	61.665	1.508
5 (SE)	118.807	62.550	1.520	14 (SH)	114.454	68.262	1.514
6 (SH)	81.294	96.419	1.789	15 (SE)	145.498	51.111	1.108
7 (SE)	159.983	46.410	1.064	16 (SH)	41.859	189.556	2.897
8 (SH)	39.412	201.300	2.730	17 (SE)	159.242	46.481	0.797
9 (SE)	195.984	37.662	1.052	18 (SH)	424.415	18.386	0.541
C_{in} (pF)	0.428			C_{out} (pF)	No		
Z_S (Ω)	50			Z_L (Ω)	53.83		

in Fig. 13. No additional tools were employed to enhance numerical stability.

The maximum achievable filter order mainly depends on *step 1* of Section II-A, as any numerical errors in the synthesis of the RC function will persist and may even grow randomly throughout the following steps, especially during element extraction. We have set the order limit to $N = 18$, which, after mapping, corresponds to $N_{\mathrm{DB}} = 38$ without inductors or $N_{\mathrm{DB}} = 40$ when considering them. This limitation arises because, when calculating Feldtkeller's equation for the RC function, it introduces too many numerical issues for orders higher than $N = 18$, which later leads to the failure of the extraction process. This maximum order can be slightly improved by using [23] in *step 1* of Section II-A.

Table V presents a comparison of the maximum achievable orders and the corresponding computation times for various FBWs using different computational methods to perform the complete extraction process. The DB methodology introduced in [13] is only capable of extracting AW filters up to fourth order for any FBW without using additional tools to enhance numerical stability. To reach higher orders while still relying on coefficient-based methods, it becomes necessary to use

TABLE V

COMPARISON OF COMPUTATIONAL METHODS FOR THE SYNTHESIS OF AW LADDER FILTERS IN THE BANDPASS DOMAIN

Computational method	Maximum order N		
	FBW = [2 - 4] %	FBW = [4 - 12] %	FBW > 12%
Coefficient-based [13]	4	6	8
Coefficient-based [13] using Symbolic Math Toolbox [25]	5	7	9
Coefficient-based [13] using Advanpix Commercial Tool [26]	7	10	18
Root-based (this work)	18	18	18
Computational method	**Computation time for the above AW filter orders N**		
	FBW = [2 - 4] %	FBW = [4 - 12] %	FBW > 12%
Coefficient-based [13]	0.035 s	0.043 s	0.052 s
Coefficient-based [13] using Symbolic Math Toolbox [25]	3.261 s	5.250 s	16.019 s
Coefficient-based [13] using Advanpix Commercial Tool [26]	7.587 s	15.94 s	87.256 s
Root-based (this work)	0.210 s	0.203 s	0.195 s

the Symbolic Math Toolbox [25] or Advanpix [26], which increase numerical precision by extending the number of digits supported by the double format. However, the tradeoff for this enhanced precision is a substantial increase in computational cost. In contrast, the proposed root-based methodology not only reduces computation time by avoiding the use of such toolboxes but also increases the achievable filter order up to 18 for any FBW. Note that the reported computation time in Table V corresponds to the maximum achievable order case ($N = 18$). This computation time is reduced to approximately 0.04–0.07 s for AW ladder filters of order 3–7.

V. CONCLUSION

This article introduces a new DB methodology that generalizes the synthesis of AW ladder filters in the bandpass domain, surpassing previous LP synthesis techniques that are based on narrowband approximations and do not account for the asymptotes at extreme frequencies in the definition of the filtering function. The proposed approach combines the strengths of current LP and DB techniques, enhancing the accuracy in synthesizing the ladder topology while maintaining standard-double precision during the entire procedure. By incorporating RC functions to address the missing in-band RZs, CRZs can be added to control the I/O phases in a frequency-dependent manner, allowing for the management of OoB fly-backs from the normalized frequency domain. To assess the effectiveness of the proposed method, a synthesized wideband AW ladder filter has been compared with a manufactured $LiNbO_3$ thin-film AW ladder filter operating from 21.35 to 25.65 GHz. The results show a perfect representation of the filtering function in the bandpass domain because it accounts for the asymptotes at extreme frequencies. Once the flexibility in the construction of transfer functions oriented to ladder networks is demonstrated, the numerical stability of the method has been validated even for narrowband filters, achieving up to order 18.

REFERENCES

[1] A. Hagelauer et al., "From microwave acoustic filters to millimeter-wave operation and new applications," *IEEE J. Microw.*, vol. 3, no. 1, pp. 484–508, Jan. 2023.

[2] A. Hagelauer, G. Fattinger, C. C. W. Ruppel, M. Ueda, K.-Y. Hashimoto, and A. Tag, "Microwave acoustic wave devices: Recent advances on architectures, modeling, materials, and packaging," *IEEE Trans. Microw. Theory Techn.*, vol. 66, no. 10, pp. 4548–4562, Oct. 2018.

[3] C. C. W. Ruppel, "Acoustic wave filter technology—A review," *IEEE Trans. Ultrason., Ferroelectr., Freq. Control*, vol. 64, no. 9, pp. 1390–1400, Sep. 2017.

[4] A. Giménez, J. Verdú, and P. De Paco Sánchez, "General synthesis methodology for the design of acoustic wave ladder filters and duplexers," *IEEE Access*, vol. 6, pp. 47969–47979, 2018.

[5] P. Warder and A. Link, "Golden age for filter design: Innovative and proven approaches for acoustic filter, duplexer, and multiplexer design," *IEEE Microw. Mag.*, vol. 16, no. 7, pp. 60–72, Aug. 2015.

[6] E. Guerrero, L. Acosta, J. Verdú, and P. de Paco, "Direct synthesis of acoustic wave multiplexers built on fully canonical multiport functions," *IEEE Trans. Microw. Theory Techn.*, vol. 71, no. 4, pp. 1391–1401, Apr. 2023.

[7] R. Ruby, "A snapshot in time: The future in filters for cell phones," *IEEE Microw. Mag.*, vol. 16, no. 7, pp. 46–59, Aug. 2015.

[8] H. Campanella, Y. Qian, C. O. Romero, J. S. Wong, J. Giner, and R. Kumar, "Monolithic multiband MEMS RF front-end module for 5G mobile," *J. Microelectromech. Syst.*, vol. 30, no. 1, pp. 72–80, Feb. 2021.

[9] J. Mateu, "Acoustic wave transversal filter for 5G N77 band," *IEEE Trans. Microw. Theory Techn.*, vol. 69, no. 10, pp. 4476–4488, May 2021.

[10] S. Cano, L. Acosta, C. Caballero, J. Verdú, and P. de Paco, "Synthesis of wideband filters based on acoustic wave transversal and ladder topologies," in *Proc. IEEE Int. Conf. Microw. Acoust. Mech.*, May 2024, pp. 101–104.

[11] G. Ariturk, N. R. Almuqati, Y. Yu, E. T.-T. Yen, A. Fruehling, and H. H. Sigmarsson, "Exact synthesis of hybrid acoustic–electromagnetic filters with wideband Chebyshev responses," *IEEE Trans. Microw. Theory Techn.*, vol. 72, no. 5, pp. 3185–3199, Oct. 2023.

[12] R. J. Cameron, C. M. Kudsia, and R. R. Mansour, *Microwave Filters for Communication Systems*. Hoboken, NJ, USA: Wiley, 2018.

[13] I. Evdokimova, J. Verdú, and P. de Paco, "Bandpass phase correction methodology for ladder-type acoustic filters," in *Proc. 48th Eur. Microw. Conf. (EuMC)*, Madrid, Spain, Sep. 2018, pp. 683–686.

[14] S. Amari, F. Seyfert, and M. Bekheit, "Theory of coupled resonator microwave bandpass filters of arbitrary bandwidth," *IEEE Trans. Microw. Theory Techn.*, vol. 58, no. 8, pp. 2188–2203, Aug. 2010.

[15] R. Zhang and L. Zhu, "Synthesis of dual-wideband bandpass filters with source-load coupling network," *IEEE Trans. Microw. Theory Techn.*, vol. 62, no. 3, pp. 441–449, Mar. 2014.

[16] I. Evdokimova, A. Gimenez, J. Verdú, and P. de Paco, "Synthesis of ladder-type acoustic filters in the band-pass domain," in *Proc. 47th Eur. Microw. Conf. (EuMC)*, Oct. 2017, pp. 640–643.

[17] H. Tian, Y. Zheng, and Y. Dong, "Synthesis of ladder-and DMS-type acoustic wave filters and duplexers in bandpass domain," *IEEE Trans. Microw. Theory Techn.*, vol. 72, no. 8, pp. 4445–4456, Jan. 2024.

[18] B. Liu, K. Li, X. Chen, P.-L. Chi, and T. Yang, "Synthesis of wideband cross-coupled resonator filter for direct circuit implementation using lumped elements," *IEEE Microw. Wireless Technol. Lett.*, vol. 33, no. 6, pp. 815–818, Jun. 2023.

[19] B. Liu, K. Li, X. Chen, P. Chi, and T. Yang, "Synthesis of wideband bandpass filter with cross-coupled or inline topology for direct circuit implementation using lumped elements," *IEEE Trans. Microw. Theory Techn.*, vol. 72, no. 1, pp. 737–749, Nov. 2023.

[20] F. Xiao, "Direct synthesis of general Chebyshev bandpass filters in the bandpass domain," *IEEE Trans. Circuits Syst. I, Reg. Papers*, vol. 61, no. 8, pp. 2411–2421, Aug. 2014.

[21] S. Amari and G. Macchiarella, "Synthesis of inline filters with arbitrarily placed attenuation poles by using nonresonating nodes," *IEEE Trans. Microw. Theory Techn.*, vol. 53, no. 10, pp. 3075–3081, Oct. 2005.

[22] M. Oldoni, S. Tamiazzo, G. Macchiarella, G. G. Gentili, and S. C. Mejillones, "Improved section extraction technique for fully-canonical filters," in *Proc. IEEE Eur. Microw. Conf.*, Sep. 2024, pp. 176–179.

[23] P. Zhao, B. Liu, M. Oldoni, and Y. Yang, "Improving accuracy in solving feldtkeller equation," *IEEE Microw. Wireless Compon. Lett.*, vol. 34, no. 3, pp. 251–254, Jan. 2024.

[24] O. Barrera et al., "Thin-film lithium niobate acoustic filter at 23.5 GHz with 2.38 dB IL and 18.2% FBW," *J. Microelectromech. Syst.*, vol. 32, no. 6, pp. 622–625, 2023.

[25] *Symbolic Math Toolbox*. Accessed: Apr. 18, 2025. [Online]. Available: https://es.mathworks.com/help/symbolic/index.html

[26] *Advanpix Multiprecision Computing Toolbox for MATLAB*. Accessed: Apr. 18, 2025. [Online]. Available: https://www.advanpix.com/

[27] M. Iwaki, T. Tanaka, M. Ueda, and Y. Satoh, "Design consideration on converged rx SAW duplexer module for multiband RF front end," *IEEE Trans. Microw. Theory Techn.*, vol. 65, no. 11, pp. 4629–4635, Nov. 2017.

[28] S. Kreuzer, A. Volatier, G. Fattinger, and F. Dumont, "Full band 41 filter with high Wi-Fi rejection–design and manufacturing challenges," in *Proc. IEEE Int. Ultrason. Symp. (IUS)*, Oct. 2015, pp. 1–4.

[29] R. Saal and E. Ulbrich, "On the design of filters by synthesis," *IRE Trans. Circuit Theory*, vol. CT-5, pp. 284–327, Dec. 1958.

[30] M. Li et al., "A fully matched LTE—A carrier aggregation quadplexer based on BAW and SAW technologies," in *Proc. IEEE Int. Ultrason. Symp.*, Sep. 2014, pp. 77–80.

[31] R. Baum, "Design of unsymmetrical band-pass filters," *IEEE Trans. Circuit Theory*, vol. CT-4, no. 2, pp. 33–40, Jan. 1957.

[32] Y. Zeng, Y. Yang, Y. Wu, M. Yu, J. Peng, and D. Liang, "Exploiting redundancy in direct synthesis for inline filters," *IEEE Trans. Microw. Theory Techn.*, vol. 69, no. 10, pp. 4489–4498, Oct. 2021.

[33] S. Tamiazzo, G. Macchiarella, and F. Seyfert, "Path filters: A class of true inline topologies with transmission zeros," *IEEE Trans. Microw. Theory Techn.*, vol. 70, no. 1, pp. 850–863, Jan. 2022.

[34] J. Verdú, M. Faura, L. Acosta, E. Guerrero, C. Caballero, and P. De Paco, "Synthesis of the double-ladder topology with arbitrary bandwidths and dual-band response," in *IEEE MTT-S Int. Microw. Symp. Dig.*, Jun. 2022, pp. 8–11.

[35] C. Caballero, L. Acosta, E. Guerrero, J. Verdú, and P. de Paco, "Nonstandard transmission responses enabling feasible microwave-acoustic ladder filters," *IEEE Trans. Microw. Theory Techn.*, vol. 71, no. 9, pp. 3712–3721, Sep. 2023.

[36] E. Guerrero, J. Verdú, and P. de Paco, "On the influence of input phase on the allocation of transmission zeros in acoustic ladder filters," in *IEEE MTT-S Int. Microw. Symp. Dig.*, Nov. 2021, pp. 102–105.

[37] G. Macchiarella, M. Oldoni, F. Seyfert, and S. Amari, "Synthesis of microwave filters with 'reactive' nodes," in *Proc. 42nd Eur. Microw. Conf.*, Oct./Nov. 2012, pp. 467–470.

[38] S. Tamiazzo and G. Macchiarella, "Synthesis of cross-coupled prototype filters including resonant and non-resonant nodes," *IEEE Trans. Microw. Theory Techn.*, vol. 63, no. 10, pp. 3408–3415, Oct. 2015.

[39] K. Hashimoto, *RF Bulk Acoustic Wave Filters for Communications*. Norwood, MA, USA: Artech House, 2009.

Santi Cano (Graduate Student Member, IEEE) was born in Sabadell, Spain, in 2000. He received the B.S. and M.S. degrees in telecommunications engineering from the Universitat Autónoma de Barcelona (UAB), Barcelona, Spain, in 2021 and 2023, respectively, where he is currently pursuing the Ph.D. degree at WavesLab Group.

His main research interests include the synthesis of microwave filters and the synthesis and design of microwave acoustic filters for wireless communications applications.

Carlos Caballero (Graduate Student Member, IEEE) was born in Santa Coloma de Gramenet, Spain, in 1997. He received the B.S. (Hons.) and M.S. degrees in telecommunications engineering from the Universitat Autónoma de Barcelona (UAB), Barcelona, Spain, in 2019 and 2022, respectively, where he is currently pursuing the Ph.D. degree at WavesLab Group.

His main research interests include the synthesis of microwave filters and the synthesis and design of microwave acoustic filters.

Omar Barrera (Senior Member, IEEE) received the B.S. degree in electrical engineering from UABC, Mexicali, Mexico, in 2009, and the M.S. degree in electrical engineering from Dongguk University, Seoul, South Korea, in 2013. He is currently pursuing the Ph.D. degree at the Department of Electrical and Computer Engineering, The University of Texas at Austin, Austin, TX, USA.

He has previous research experience in antennas and RF circuits. He also has industry experience in the automotive industry, where he worked as a Manufacturing Engineer. His current research interests involve microwave and mm-wave devices and circuits, in particular, the development and characterization of acoustic filters for new radio mobile applications.

Mr. Barrera was a recipient of an Outstanding Student Oral Presentation Award Finalist at IEEE MEMS 2024 and was awarded second place in the Conference Paper Award at the IEEE International Microwave Filter Workshop (IMFW 2024). He has also received a number of awards, including the Cadence Diversity in Technology Scholarship in 2023.

Ruochen Lu (Senior Member, IEEE) received the B.E. degree (Hons.) in microelectronics from Tsinghua University, Beijing, China, in 2014, and the M.S. and Ph.D. degrees in electrical engineering from the University of Illinois at Urbana-Champaign, Urbana, IL, USA, in 2017 and 2019, respectively.

He is an Assistant Professor with the Department of Electrical and Computer Engineering, The University of Texas at Austin, Austin, TX, USA. His works aim to demonstrate RF MEMS platforms, toward higher operating frequencies, and more efficient transduction between the EM and acoustics. In addition, he works on ultrasonic transducers and multiphysics hybrid microsystems for signal processing, sensing, and computing applications. His research primarily focuses on developing chip-scale acoustic and electromagnetic components and microsystems for RF applications.

Dr. Lu received the IEEE MTT-S Microwave Award in 2022, the IEEE Ultrasonics Early Career Investigator Award in 2024, and the NSF Career Award in 2024. Along with his students, he received the Best Student Paper Awards at the IEEE International Frequency Control Symposium (IFCS) 2017 and 2023, the IEEE International Ultrasonics Symposium (IUS) 2018 and 2022, the IEEE International Conference on Microwave Acoustics and Mechanics (IC-MAM) 2022, and the third place Best Student Paper Award at the IEEE International Microwave Symposium (IMS) 2024. He received the Junior Faculty Excellence in Teaching Award from The University of Texas at Austin in 2024.

Jordi Verdú (Senior Member, IEEE) was born in Sabadell, Spain. He received the M.S. degree in telecommunication engineering and the Ph.D. degree (cum laude) from the Universitat Autónoma de Barcelona (UAB), Barcelona, Spain, in 2006 and 2010, respectively.

From 2006 to 2010, he was a Member of WavesLab Group. In 2010, he joined the RF System Group, European Spallation Source in Bilbao (ESS-B), Bilbao, Spain, as a Group Coordinator. From 2011 to 2012, he was at the École Polytechnique Fédérale de Lausanne, Lausanne, Switzerland, through a Marie Curie grant. In 2013, he joined the Theory Signal Communication Group, Universitat Politócnica de Catalunya, Barcelona. He is currently an Associate Professor at the Universitat Autónoma de Barcelona, where he teaches microwave engineering courses. He has been extensively working on linear modeling of acoustic wave devices and new synthesis techniques and advanced configurations for acoustic wave filters. His current research interests include the design of microwave devices and linear modeling, but also the design of active devices for space applications.

Dr. Verdú is a member of WavesLab Group. He received the Department Best Thesis Prize for his Ph.D. degree. He is the Vice-Chair of the MTT-6 MEMS and Microwave Acoustics Technical Committee.

Pedro de Paco (Senior Member, IEEE) was born in Badalona, Spain. He received the M.S. degree in telecommunication engineering and the Ph.D. degree (cum laude) from the Universitat Politècnica de Catalunya (UPC), Barcelona, Spain, in 1997 and 2003, respectively.

In 1998, he joined the Electromagnetic and Photonics Engineering Group (EEF), Signal Theory and Communications Department (TSC), UPC, with a grant from the Institut d'Estudis Espacials de Catalunya (IEEC), Barcelona, in a joint activity related with European Scientific Space Mission Planck, Noordwijk, The Netherlands. He was a member of the LFI-Radiometer Working Group and the Planck Consortium. During his Ph.D., he has participated in several national and international research projects mostly related to microwave and millimeter-wave circuits and systems applied to the design and testing of remote sensing instruments and front-end point-to-multipoint broadband communication systems. Since 2004, he has been an Associate Professor with the Universitat Autónoma de Barcelona (UAB), Barcelona, where he teaches applied electromagnetics and microwave engineering courses. From 2010 to 2013, he was the Deputy Director and a member of the Executive Board of the Department of Telecommunication and System Engineering, UAB. From 2018 to 2019, he was a Visiting Researcher with the Microwave and RF Research Group, University of Colorado at Boulder, Boulder, CO, USA. He has advised eight Ph.D. students. His main research interests include microwave filter synthesis, microwave acoustics filter synthesis and design, and microwave and radar systems and devices.

Dr. de Paco is a member of the MTT-6 RF MEMS and Microwave Acoustics Committee. He was awarded three times with merits in research and recognized with merits in University training by l'Agència de Qualitat, and Advanced Research by Generalitat de Catalunya. He is a reviewer of IEEE TRANSACTIONS ON MICROWAVE THEORY AND TECHNIQUES and IEEE MICROWAVE AND WIRELESS COMPONENTS LETTERS. He serves as a member of the Technical Review Board for the European Microwave Conference. He has been appointed as a Technical Expert for Telecommunications Equipment by the National Agency of Accreditation.